F. F. CHEN

PROCEEDINGS OF THE JAPAN-U.S. SEMINAR ON

THEORY AND APPLICATION OF MULTIPLY-IONIZED PLASMAS PRODUCED BY LASER AND PARTICLE BEAMS

Nara Hotel
Nara, Japan
May 3-7, 1982

Edited by
Chiyoe YAMANAKA

INSTITUTE OF LASER ENGINEERING
OSAKA UNIVERSITY
1982

Francis F. Chen, Chan Joshi, Christopher E. Clayton
Behrouz Amini, and Hugh C. Barr

University of California, Los Angeles, California 90024

I. INTRODUCTION

In this paper we present recent results obtained in the Laser Interaction Laboratory, Electrical Engineering Department, UCLA, in an ongoing program to study nonlinear plasma phenomena which can occur in the underdense regions of the blow-off corona of inertial fusion targets. The driver used is a 50-J CO_2 oscillator-amplifier system with triple-pass Cassegrain optics in the final stage. In the work given here, the laser was gain-switched, giving a 50-nsec FWHM pulse with maximum intensity $I_o \lesssim 5 \times 10^{11}$ W/cm^2 when focused with an f/7.5 lens. To ensure the absence of a critical layer ($n = n_c$, $\omega_o = \omega_p$) and of a quarter-critical layer ($n = n_c/4$, $\omega_o = 2\omega_p$), two types of plasma targets were used. The first is a high-current arc giving an $n_e \simeq 5 \times 10^{16}$ cm^{-3}, $T_e \simeq T_i \simeq 5$ eV partially ionized plasma in various gases; the focal region can be further ionized and heated by the first part of the incident laser pulse[1]. The second source is a fast, 6-kJ theta pinch, 7.5 cm in diameter and 25 cm long, which provides fully ionized plasmas in the 10^{16} – 10^{18} cm^{-3} density range, with an nT_e product of $\simeq 3 \times 10^{18}$ cm^{-3} eV. With both these targets, there is no laser breakdown and no scattering unless the discharge is fired.

II. FILAMENTATION

Although it is predicted to occur with a low threshold, filamentation of laser light into self-focused channels devoid of plasma is almost never seen, because it does not leave a telltale tracer of frequency-shifted scattered light. We have found a sensitive method to detect the density modulations associated with either thermal or ponderomotive self-focusing or filamentation. The experimental set-up is shown in Fig. 1. The CO_2 pump beam is focused into a 25-Torr hydrogen arc plasma with $n_e \simeq 10^{18}$ cm^{-3}. A ruby-laser probe beam is directed across the density channels, which cause a phase modulation of the wavefront. The unmodulated light is blocked at the focus of a Fourier transform lens, and a spatial filter further suppresses k-components outside the range of interest. The remaining light is focused by

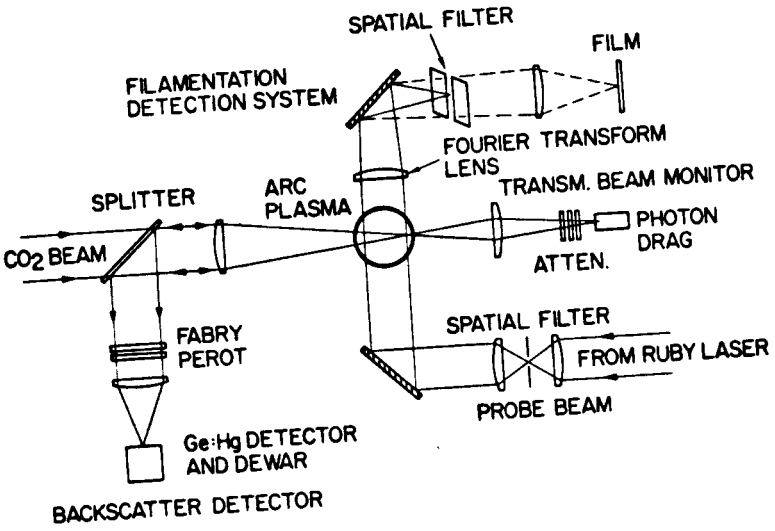

Fig. 1

another lens onto film, on which a direct image of the density striations can be recorded. An example is shown in Fig. 2b. Density variations of 200-μm width can be seen near the focus of the pump beam. The other marks are from a constant background of stray light, as shown in Fig. 2a, which was taken with the CO_2 beam off. The degree of phase modulation is consistent with slab perturbations with $\Delta n = 8 \pm 4 \times 10^{16}$ cm^{-3}. The transmitted light shows a period of diminished absorption in coincidence with the appearance of filamentation. Further details have been published[2]. This technique will allow the predictions of filamentation theory to be checked experimentally.

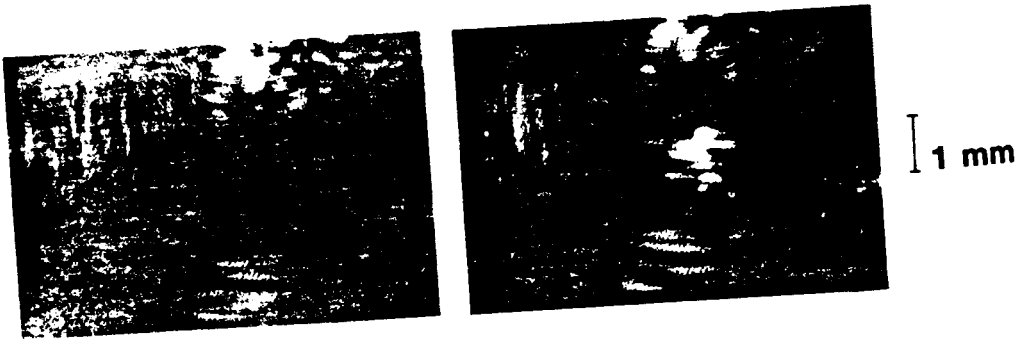

(a) (b)

Fig. 2

III. RESONANT SELF-FOCUSING

When one uses a multi-line driver either to gain efficiency or to suppress parametric instabilities, there is a danger that the beat frequency $\Delta\omega$ between two lines will excite plasma waves at the layer where $\Delta\omega \simeq \omega_p$. We have found experimentally that this effect is surprisingly strong and results in anomalous refraction and defocussing of the incident light. The apparatus is shown in Fig. 3. A weak pump beam from the oscillator alone is sent into the arc plasma, and the forward scattered light between 5 and 12^o half-angle is collected by a lens and detected in an infrared spectrometer. By varying the pressure in an SF_6 cell, one can cause the oscillator to produce the 9.55-μm and 10.26-μm lines with intensity ratios from 10 to > 10^6. When the

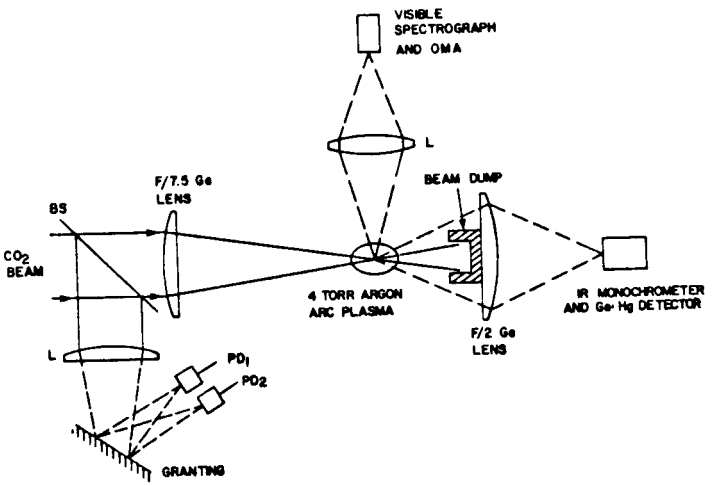

Fig. 3

density in the arc reaches 5.8×10^{16} cm^{-3}, at which ω_p matches the $\Delta\omega$ of these two lines, the forward scattered light increases almost 5 orders of magnitude over stray light. The raw data are shown in Fig. 4, and the density resonance is more clearly shown (on a linear scale) in Fig. 5. The density is measured by ruby-laser interferometry. Although the ω_p condition strongly indicates the excitation of a plasma wave, there was no measurable red- or blue-shift of the scattered light. This was determined by varying the intensity ratio and, most conclusively, by detecting a weak, non-resonant 10.6-μm line. This refraction effect has an extremely low threshold and saturation value of I_o, as shown in

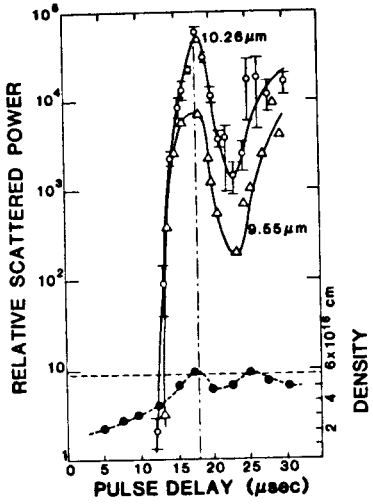

Fig. 4

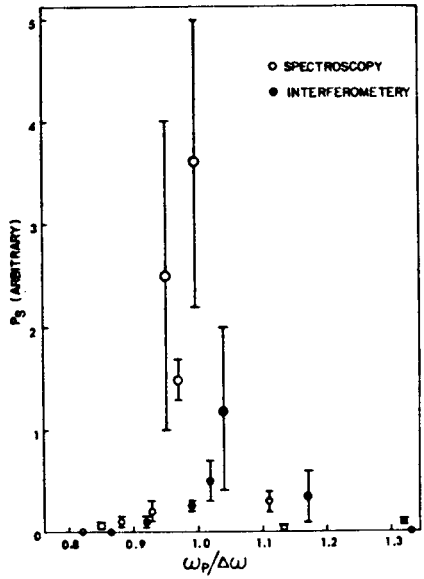

Fig. 5

Fig. 6. Direct detection of the plasma wave was not possible, but we did observe a scattered line near 11.0-μm, shown in the inset of Fig. 6, which is interpreted as Thomson scattering of the 10.26-μm line from a plasma wave. The intensity of this line indicates a saturation amplitude $n_1/n_o \simeq 1\%$ for the plasma wave, a level that is easily reached by optical mixing if the incident lines have equal amplitude. If the 10.26-μm line is weaker than the 9.55-μm line, the plasma wave is driven up by forward Raman scattering. Fig. 7 shows that the saturation amplitude is reached when $I_o(10.26)$ is only 1% of $I_o(9.55)$. Further details have been published[3].

To explain these observations, we have extended the theory of self-focusing[4] to the case where the ponderomotive force F_{NL} of the light is supplemented by the F_{NL} of the resonantly excited plasma wave. It turns out that F_{NL} is enhanced by the ratio $A = (n_1/n_o)^2/(v_o/c)^2$, where v_o is the quiver velocity of the incident beam. For $n_1/n_o = 0.01$ and $I_o = 10^{10}$ W/cm^2, A is of order 10^2, so that a low threshold of self-focusing can be expected. If the nonlinear equations for self-focusing are numerically integrated to give the relative beam width f vs. distance z, one sees in Fig. 8 that there is a shift Δz in the focal point,

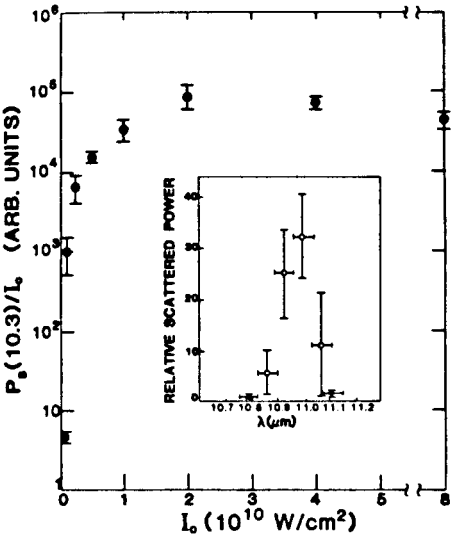

Fig. 6

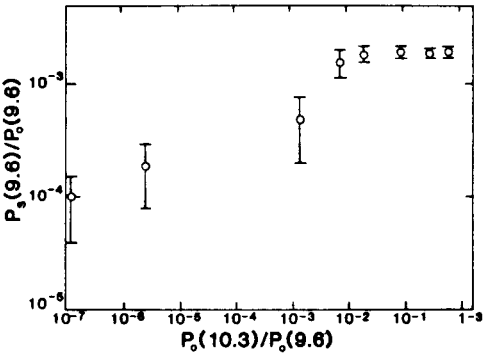

Fig. 7 (top)

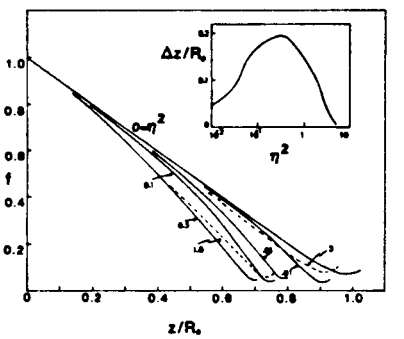

Fig. 8

which in an inhomogeneous plasma can cause refracted light to miss the beam dump. The shift Δz reaches a maximum as $\eta^2 = v_o^2/4v_{th}^2 \propto F_{NL}$ is increased, and then it decreases to zero (its vacuum value) if one evacuates the channel by applying very large values of η^2. This maximum correctly predicts[3] the observed saturation at $I_o \simeq 10^{10}$ W/cm^2.

IV. STIMULATED BRILLOUIN SCATTERING

1. Thomson scattering. In earlier work we have confirmed the linear growth of SBS from thermal noise[5], unraveled sidescatter signals[6], measured its saturation level[7], and checked its dependence on focusing f-number, target Z, and single-modedness of the pump[8]. Our recent work has been directed at the remaining problems of why SBS occurs in short spikes and why it saturates at < 10% in our experiments.

To probe the behavior of the ion wave, we have used a 1-J, 30-nsec ruby laser pulse to do collective Thomson scattering from it. For backscatter with $n << n_c$, the propagation constant of the ion wave is fixed at $k_i \simeq 2k_o = 11{,}900$ cm^{-1}. If the probe beam $\underline{k}_{ru}$ is perpendicular to $\underline{k}_i$, the scattering angle is given by $\underline{k}_s = \underline{k}_{ru} \pm \underline{k}_i$, or $\pm \tan\theta = k_i/k_{ru} = \lambda_{ru}/\lambda_i = 0.69/5.3 = 0.13$, so that θ is fixed at $\pm 7.5^o$. The scattering parameter $\alpha = 1/k_i\lambda_D$ is about 10 for $n \simeq 2 \times 10^{17}$ cm^{-3}, $T_e \simeq 20$ eV.

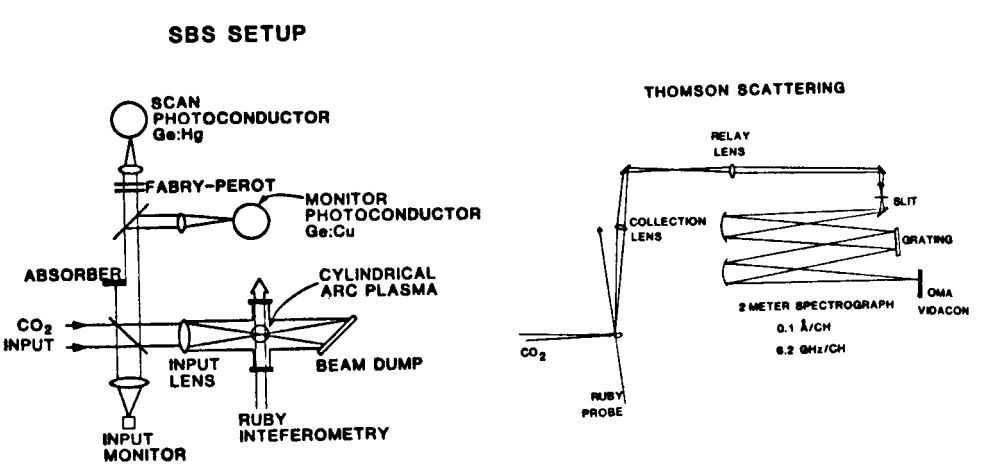

Fig. 9

The set-up for 7.5° forward scattering of ruby light and 180° backscatter of CO_2 light is shown in Figs. 9(a) and (b). The backscatter detection is as usual; the forward scattered ruby light is dispersed by a grating and recorded by an optical multichannel analyzer (OMA). The resolution of the OMA is such that the stray light peak occupies three channels. The scattered light is clearly red- or blue-shifted (depending on whether θ is - or + 7.5°) by two channels, corresponding to ω_i = 9-12 GHz, in agreement with the measured SBS redshift.

We first checked the $\underline{k}_i$ spectrum by varying the scattering angle θ. The scattered ruby light was sharply collimated within ¼° of 7½° (FWHM), showing that the acoustic wave is sharply collimated along $\underline{k}_o$, in agreement with observations on optical ray retracing of SBS. Next, we probed the spatial variation of the acoustic wave amplitude by shifting the focal position of the CO_2 laser relative to the Thomson scattering system. Fig. 10 shows the radial variation, and Fig. 11 the axial variation. In Fig. 11, the amplitude is seen to grow experimentally toward the laser (to the left), in agreement with the picture[9] of highly Landau-damped ion waves which do not convect appreciably in the forward direction. The amplitude behavior at the left of Fig. 11 is not completely understood;

it could be caused by convection of wave energy into the region where the pump is defocused or by the excitation, in the weak-pump region, of SBS seeded by backscatter from the strong-pump region.

Correlation between Thomson scatter and the occurrence of an SBS spike is observed in N_2 discharges. In Fig. 12 we show that the Thomson-scattered light increases with the SBS amplitude. Note that exact correspondence is not expected because the ruby probe is local, while the SBS signal is integrated over z. Fig. 13 shows that the Thomson-scattered light exhibits exponential growth and saturation as I_o is increased, in the same manner as the backscattered CO_2 light (dashed curve). In lighter gases such as H_2, neither the time behavior of the Thomson scatter nor its amplitude corresponded as well with the SBS signals, presumably because the propagation of ion waves away from the maximum amplitude point occurs fast enough to complicate the spatial amplitude variation at any given time. We shall need to understand the amplitude distribution before using it to throw light on the saturation mechanism.

2. Calculations of saturation. Though SBS from solid targets and in microwave experiments seems to saturate at levels predicted by ion heating[10], gas target experiments with CO_2 lasers are not so easily explained. Among these, there is disagreement among groups in the U.S.[7,11],

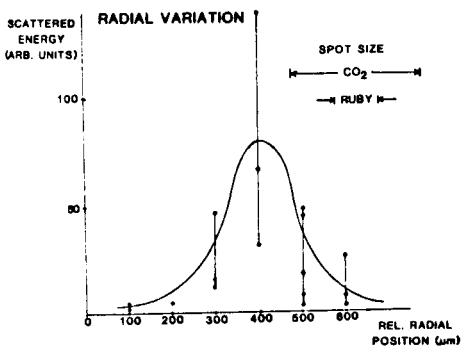

Fig. 10

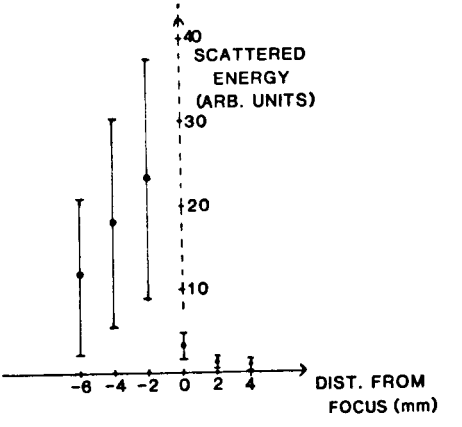

Fig. 11

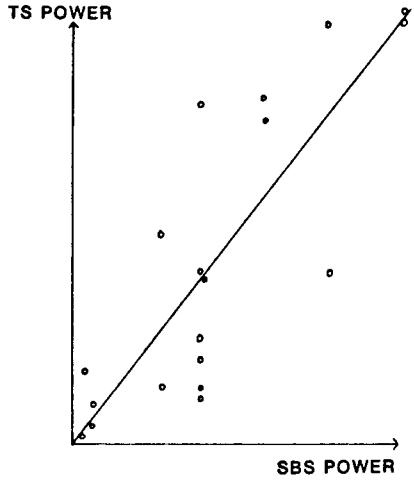

Fig. 12

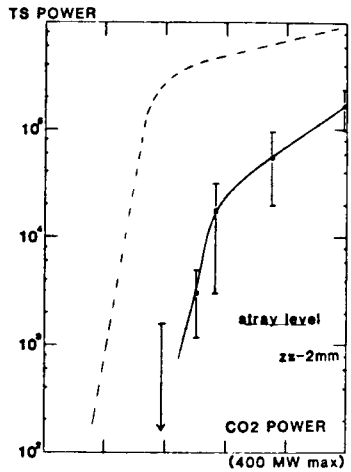

Fig. 13

which report reflectivities R ≃ 1-10%, and those in Canada[12] and Germany[13], which report R as high as 100%. We have checked[8] that using a fast lens could not produce the high reflectivities seen by others. The density difference among experiments, we feel, is the important factor. The Bragg scattering formula[9]

$$R = \frac{P_s}{P_o} = \left(\frac{\pi}{2}\frac{L}{\lambda_o}\frac{\tilde{n}}{n}\frac{n}{n_c}\right)^2 \qquad (1)$$

shows that $n = 10^{17}$ cm^{-3} and $n = 10^{18}$ cm^{-3} would give R's differing by a factor of 100 if $\tilde{n}/n$ is saturated at the same value. The mechanism that limits $\tilde{n}/n$ has been conjectured to be ion trapping[7], but we are far from establishing this as a fact.

To see just how far the gas-target results are from the ion heating limit, we have computed this limit as it applies to the UCLA[7] and Bochum[13] experiments. We start with Kruer's formulas[14] for convective SBS in the highly damped regime including pump depletion:

$$R(1-R) = B[e^{g(1-R)} - R] \qquad (2)$$

$$g = \frac{k_o L}{8} \frac{v_o^2}{v_e^2} \frac{\delta}{1-\delta} \left[\frac{\gamma_s}{\omega_s} (1+3\theta) \right]^{-1} \qquad (3)$$

where B is the initial noise level, L is the interaction length, δ is n_o/n_c, v_e^2 is KT_e/m, θ is T_i/ZT_e, and γ_s and ω_s are the ion wave damping rate and frequency. It is critical to approximate γ_s/ω_s accurately, since ion-heating saturation depends on exponential change in γ_s. Because electrons and ions equilibrate rapidly at high densities, laser experiments usually have $0.1 < \theta < 1$, exactly the range where asymptotic expressions for γ_s/ω_s fail. We have found a simple analytic fit to the exact value of γ_s/ω_s as given by the plasma dispersion function for the range $0.1 < \theta < 1$:

$$\gamma_s/\omega_s = 1.1\ \theta^{7/4} e^{-\theta^2} . \qquad (4)$$

The electron temperature is determined by the balance between inverse bremsstrahlung heating and radial heat conduction, a problem solved in Ref. 5. The result is

$$T_e \simeq 50\ n_{17}^{2/5}\ (I_{10}S)^{1/5} \quad \text{eV}, \qquad (5)$$

where n_{17} is n_o in units of 10^{17} cm^{-3}, I_{10} is I_o in units of 10^{10} W/cm^2, and S is the focal area πa^2. Conduction to ions is unimportant. The ion temperature is, similarly, determined by the balance between radial heat conduction (not axial, as in Ref. 14) and heating at the rate $(\omega_s/\omega_o)RI_o$ given by the Manley-Rowe relation[14]. Accounting for the finite initial temperature T_o, we find T_i in eV to be given by

$$T_i^2(T_i - T_o) = 3.6 \times 10^5 (a^2/L) R I_{10}. \qquad (6)$$

Eqs. (2) to (6) can be solved simultaneously on a programmable hand calculator. The results are shown on Fig. 14, as compared with the corresponding experimental data (only a few of the Bochum points are shown). It is seen that in both cases the linear growth region agrees with theory, but that saturation occurs well below the values of R predicted by the ion-heating limit. It is as if a delicate saturation mechanism limits R to 5-10%, and that this limit can be overcome at the

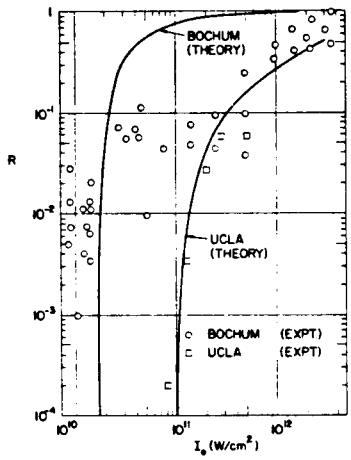

Fig. 14

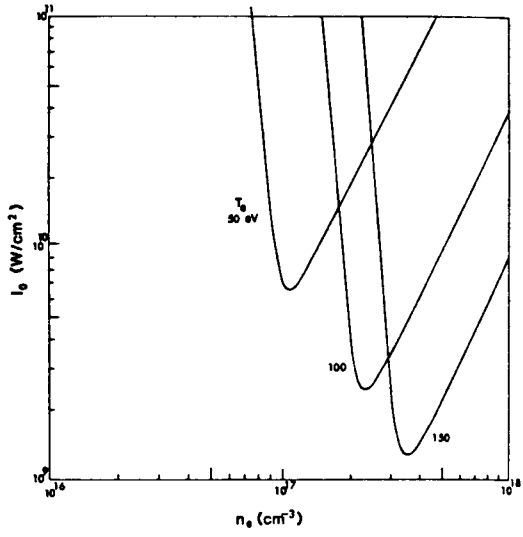

Fig. 15

highest intensities, where R can reach the nearly 100% values predicted by ion heating and pump depletion.

V. STIMULATED RAMAN SCATTERING

Excitation of plasma waves by the SRS process can lead to trapping and acceleration of electrons. In backscatter from pellet coronas, fast electrons are produced which can preheat the core. In forward scatter, the trapped electrons travel at nearly the velocity of light, and this effect can be used to make very compact accelerators[15]. Redshifted light attributed to SRS has been seen in solid target experiments, and the existence of accelerated electrons has also been confirmed[16]. Studies of SRS from underdense plasma targets, however, are rare and baffling. Watt et al.[17] have measured the spectrum of SRS backscatter from a theta-pinch similar to ours, with $n \simeq 2 \times 10^{16}$ cm^{-3} and $I_o \simeq 10^9$ W/cm^2. However, such a low threshold is possible only in infinite, homogeneous plasmas; the finite focal depth should have required much higher I_o. Offenberger et al.[18] have also reported seeing SRS, but only under peculiar circumstances. SRS was observed not in the peak of the CO_2 laser pulse but only during bursts of intensity in the tail, these bursts arising from Brillouin backscatter feedback into the laser chain.

We have attempted to produce SRS with axial incidence into the theta-pinch described in Sec. I. The CO_2 beam is focused by an f/7.5 ZnSe lens and absorbed after traversing the plasma once. The backscatter is collected by a beamsplitter in the usual fashion and detected by an IR spectrometer and a Ge:Cu photoconductor. The input has been operated at 10.6-μm to produce Raman backscatter near 11.6-μm, and at 9.6-μm to produce backscatter near 10.6-μm. In both cases strong Brillouin scatter is seen, but so far no SRS larger than $10^{-6}I_o$ has been detected. We regard this negative result as an important one obtained only after careful work, and we are trying to understand it.

The damping threshold computed from the formula[19]

$$2\gamma_o > \left(\frac{\gamma_1}{V_1} + \frac{\gamma_2}{V_2}\right)(V_1V_2)^{\frac{1}{2}} \tag{7}$$

is shown in Fig. 15. Here γ_o is the homogeneous SRS growth rate, γ_1 and γ_2 are the damping rates, and V_1 and V_2 the group velocities of the plasma and backscattered waves, respectively. For γ_1 we take the sum of the Landau damping rate and the electron-ion collisional damping rate. For each T_e, there is a sharp minimum in required I_o between the two damping regimes. With $T_e \simeq 50$ eV and $I_o = 3-5 \times 10^{11}$ W/cm^2, we should have been above threshold. When the density is inhomogeneous with scale length L_n, the further condition[19] $v_o^2/c^2 > 2/k_oL_n$ has to be satisfied. Since $dn/dz = 0$ at the midplane of the pinch, the corresponding expression[19] for a quadratic density profile has to be used. We believe that we should have exceeded also the inhomogeneous threshold.

Recalling that SBS is always strong in spite of $T_e \simeq T_i$ in the pinch, we believe that the usual predictions of convective and absolute, homogeneous and inhomogeneous thresholds for SRS are irrelevant. What we must consider is SRS in the presence of a density ripple with $k \simeq 2k_o$ created by SBS, and we sketch here our theoretical work on this problem. The plasma and backscattered waves are described by the coupled mode equations

$$\ddot{n}_1 + \omega_p^2(x)n_1 - 3v_e^2n_1'' = n_o(v_ov_2)'' \tag{8}$$

$$\ddot{v}_2 + \omega_p^2(x)v_2 - c^2v_2'' = -v_o\omega_p^2n_1/n_o \ , \tag{9}$$

where we take $\omega_p^2(x) = (4\pi n_o e^2/m)(1 + \varepsilon \cos 2k_o x)$. Defining $z = k_o x$, $y = n_1/n_o$ and neglecting the effect of ε on propagation of wave 2, we obtain Mathieu's equation

$$y'' + (a - 2q \cos 2z)\, y = 0 \ , \tag{10}$$

where

$$a = (\omega^2 - \omega_p^2)(3k_o^2 v_e^2 + \Delta^2)^{-1} \ , \tag{11}$$

and

$$q = \tfrac{1}{2}\varepsilon\omega_p^2(3k_o^2 v_e^2 + \Delta^2)^{-1} \ , \tag{12}$$

Δ being a small frequency shift due to the ponderomotive force. The Mathieu problem has previously been treated by Kaw et al.,[20] but only when there is no driver and when k_1 is not resonant with the k of the ripple.

There are two competing effects introduced by the ripple. Solutions of Eq. (10) naturally divide themselves into those for small q and those for large q. Small q means that the variation in $\omega_p^2(x)$ can be compensated by a change in k in the dispersion relation $\omega^2 = \omega_p^2 + 3k_1^2 v_e^2$. Consequently, the plasma wave is not sinusoidal, but it exists over the whole region. Large q means that the $3k_1^2 v_e^2$ term is too small, and therefore plasma waves are trapped in the troughs of the density ripple. In the small q case, the main effect is the reflection of wave energy by the grating formed by the ripple, and therefore there is a tendency toward absolute instability. In the large q case, which we have not yet investigated, the main effect may be the channeling of energy into higher-k harmonics, which have large Landau damping and suppress the instability.

To treat the damping correctly, Eqs. (8) and (9) have been replaced by their counterparts derived from the Vlasov equation. The small-q case must be taken in order that the k-spectrum can be truncated. As usual, frequency and k-matching is most easily done with a wave with $\underline{k}_1 \simeq 2\underline{k}_o$. This wave beats with the $2k_o$ of the ripple to produce a wave with $k \simeq 0$, and this in turn generates a wave with $\underline{k}_1 \simeq -2\underline{k}_o$. Further coupling produces $\underline{k}_1 = \pm 4\underline{k}_o$, and the spectrum is terminated there. When the frequency ω_2 is such that the frequency mismatch with the $-2\underline{k}_o$

mode is finite, both modes can be excited with nearly equal amplitudes, as in a standing wave. Extending the analysis to the case of a finite region of interaction, we obtain a new instability criterion which depends on the ripple amplitude ε.

This work was supported by DOE contracts DE-AS08-81DP40135 and 40163, and NSF grants ECS 80-03558, ENG 75-16610, and ENG 77-17861.

REFERENCES

1. M. J. Herbst, C. E. Clayton, W. A. Peebles, and F. F. Chen, Phys. Fluids 23, 1319 (1980).
2. C. Joshi, C. E. Clayton, A. Yasuda, and F. F. Chen, J. Appl. Phys. 53, 215 (1982).
3. C. Joshi, C. E. Clayton, and F. F. Chen, Phys. Rev. Letters 48, 874 (1982); UCLA PPG-537 (1981), unpublished.
4. C. E. Max, Phys. Fluids 19, 74 (1976).
5. J. J. Turechek, and F. F. Chen, Phys. Fluids 24, 1126 (1981).
6. M. J. Herbst, C. E. Clayton, and F. F. Chen, J. Appl. Phys. 51, 4080 (1980).
7. M. J. Herbst, C. E. Clayton, and F. F. Chen, Phys. Rev. Letters 43, 1591 (1979).
8. C. E. Clayton, C. Joshi, A. Yasuda, and F. F. Chen, Phys. Fluids 24, 2312 (1981).
9. F. F. Chen Proceedings of the 1980 Int'l Conference on Plasma Physics, Nagoya, Japan, II, 345 (1980).
10. D. W. Phillion, W. L. Kruer, and V. C. Rupert, Phys. Rev. Letters 39, 1529 (1977).
11. Z. A. Pietrzyk and T. N. Carlstrom, Appl. Phys. Letters 35, 681 (1979).
12. A. Ng, L. Pitt, D. Salzmann, and A. A. Offenberger, Phys Rev. Letters 42, 307 (1979).
13. J. Handke, S.A.H. Rizvi, and B. Kronast, Appl. Phys. 25, 109 (1981).
14. W. L. Kruer, Phys. Fluids, 23, 1273 (1980).
15. T. Tajima and J. M. Dawson, Phys. Rev. Letters 43, 267 (1979).
16. C. Joshi, T. Tajima, J. M. Dawson, H. A. Baldis, and N. A. Ebrahim, Phys. Rev. Letters 47, 1285 (1981).
17. R. G. Watt, R. D. Brooks, and Z. A. Pietrzyk, Phys. Rev. Letters 41, 170 (1978).
18. A. A. Offenberger, R. Fedosejevs, W. Tighe, and W. Rozmus, private communication (1981 preprint).
19. C. S. Liu, M. N. Rosenbluth, and R. B. White, Phys. Fluids 17, 1211 (1974).
20. P. K. Kaw, A. T. Lin, and J. M. Dawson, Phys. Fluids 16, 1967 (1973).